Electronic Supplementary Material (ESI) for RSC Advances.

Supporting Information

$Co_2O_3/Co_2N_{0.67}$ nanoparticles encased in honeycomb-like N, P, O-codoped carbon framework derived from corncob as efficient ORR electrocatalysts

Yanling Wu[1,*], Qinggao Hou[1], Fangyuan Qiu[1], Meili Qi[1], Cuicui Sun[1], Yanli Chen[2,*]

[1] *School of Transportation and Civil Engineering, Shandong Jiaotong University, Ji'nan 250357, China;*
[2] *College of Science, China University of Petroleum (East China), Qingdao 266580, China;*
** Corresponding author, E-mail: wuyanling621@163.com*

Material characterization.

Laboratory powder X-ray diffraction patterns were collected for the samples on a Rigaku Ultima IV X-ray diffractometer with Cu Kα source (40 kV, 40 mA). The morphology and structure of the samples were observed on field-emission scanning electron microscope (SEM, Quant 250FEG) equipped with energy-dispersive X-ray (EDX) detector and high-resolution transmission electron microscopy at an acceleration voltage of 200 kV (TEM, JEM-2100F). Micromeritics Belsorp-max analyzer was applied to measure the Brunauer Emmett Teller (BET) surface area and pore size distribution (PSD). X-ray photoelectron spectroscopic (XPS) measurements were conducted on an Axis Ultra instrument from Kratos using monochromatic Al Kα radiation. Raman scattering spectra were recorded on a laser Raman microscope system (Nanophoton RAMANtouch) with an excitation wavelength of 532 nm.

Electrochemical measurements

All electrochemical measurements were carried out by using a standard three-electrode configuration on a Gamry (RDE710) electrochemical workstation, where the Ag/AgCl (KCl-saturated) electrode and a carbon rod were used as reference and counter electrodes, respectively. To ensure the repeatability of the experiment, the working electrode for each of the four catalysts was prepared by using under uniform condition. The procedure for the preparation of a working electrode was as following: the catalyst powder (5 mg) was dispersed in 0.8 mL of ethyl alcohol with 40 μL of Nafion solution (5 wt %, Sigma-Aldrich) under sonication to obtain a homogeneous suspension. Then, the catalyst ink (10 μL, 0.30 $mg \cdot cm^{-2}$) was droped on the glass carbon electrode surface. For ORR tests, Cyclic voltammetry (CV) curves were collected in a N_2-saturated or O_2-saturated

0.1 M KOH electrolyte at a scan rate of 50 $mV \cdot s^{-1}$. Additionally, the activity for ORR was also evaluated *via* the RDE method by LSV from 0.2 to 1 V in O_2-saturated 0.1 M KOH electrolyte. The ORR stability in O_2-saturated 0.1 M KOH solution was tested by current versus time (i-t) test with a rotating speed of 1600 rpm. The ORR performance of the as-prepared catalysts were make a comparison with the state-of-the-art commercial Pt/C (20 wt%) electrocatalyst (HiSPEC®3000, Alfa Aesar).

Supplementary figures

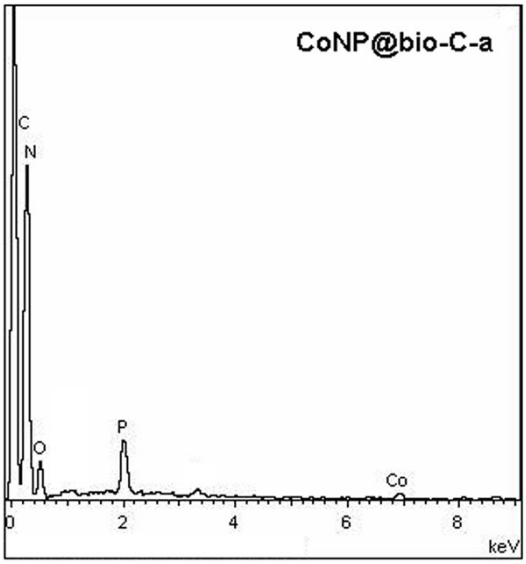

Figure S1. The EDS image of CoNP@bio-C-a.

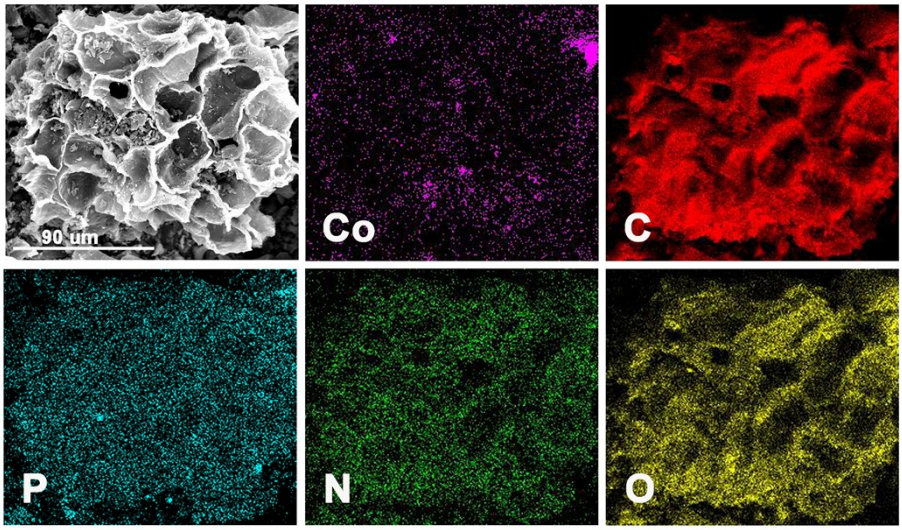

Figure S2. SEM image of CoNP@bio-C-a used in the EDS mapping area revealing the elemental distribution of Co, C, P, N, and O.

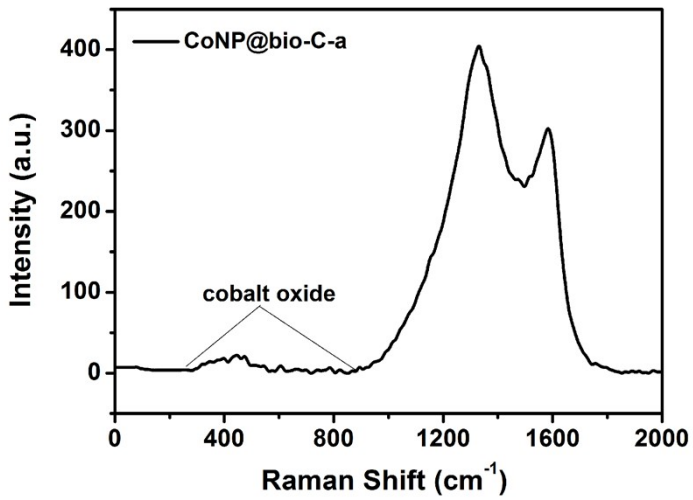

Figure S3. Raman spectrum of the as-prepared CoNP@bio-C-a.

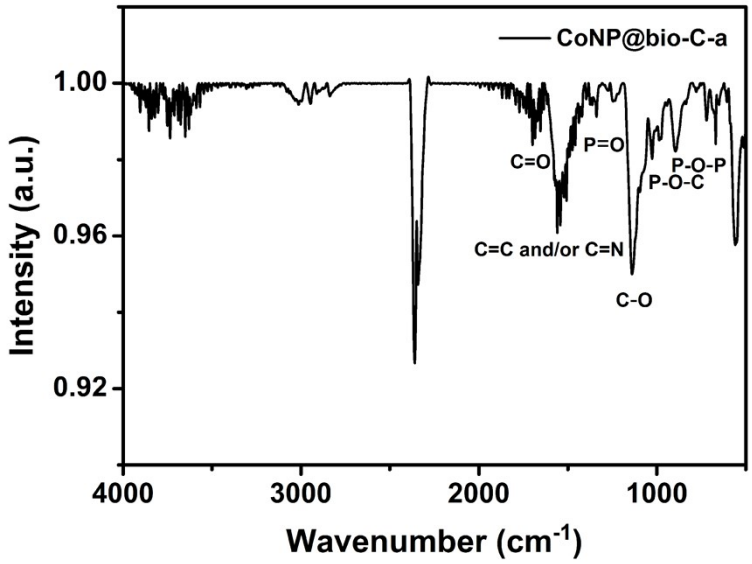

Figure S4. FT-IR spectrum of the as-prepared CoNP@bio-C-a.

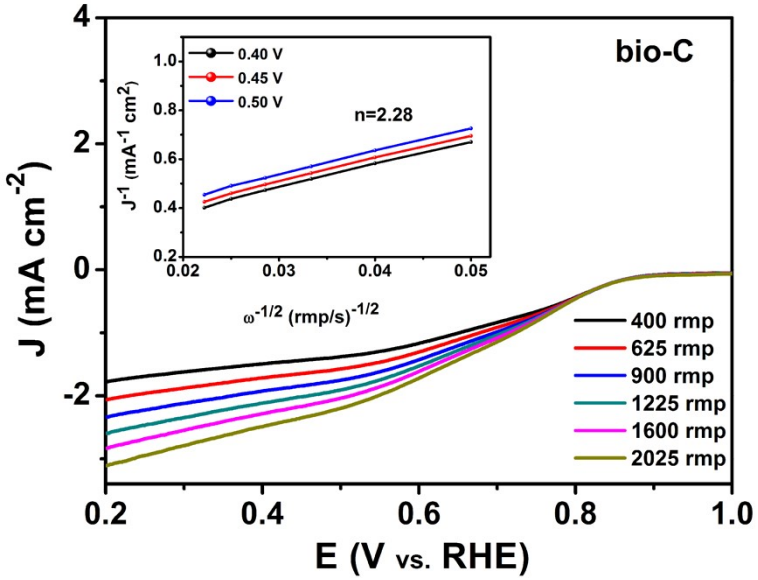

Figure S5. LSV curves of bio-C at various rotating speeds, respectively. (Inset: K–L plots of bio-C at various potentials.)

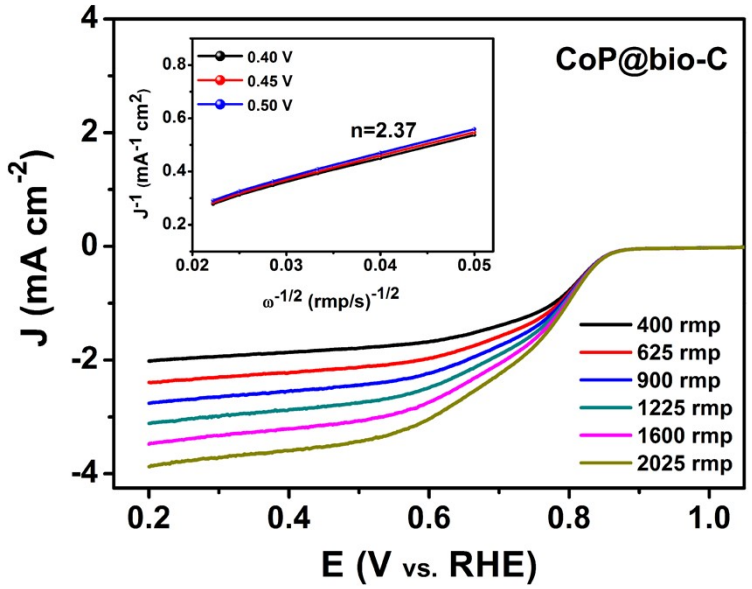

Figure S6. LSV curves of CoP@bio-C at various rotating speeds, respectively. (Inset: K–L plots of CoP@bio-C at various potentials.)

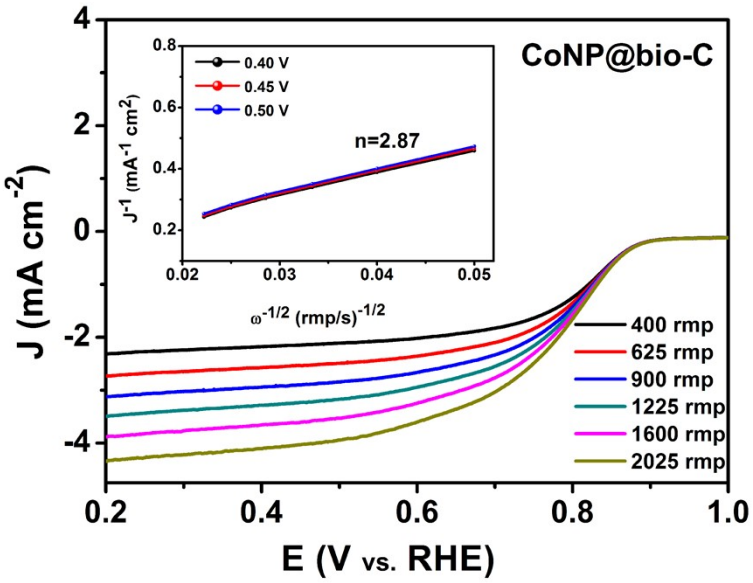

Figure S7. LSV curves of CoNP@bio-C at various rotating speeds, respectively. (Inset: K–L plots of CoNP@bio-C at various potentials.)

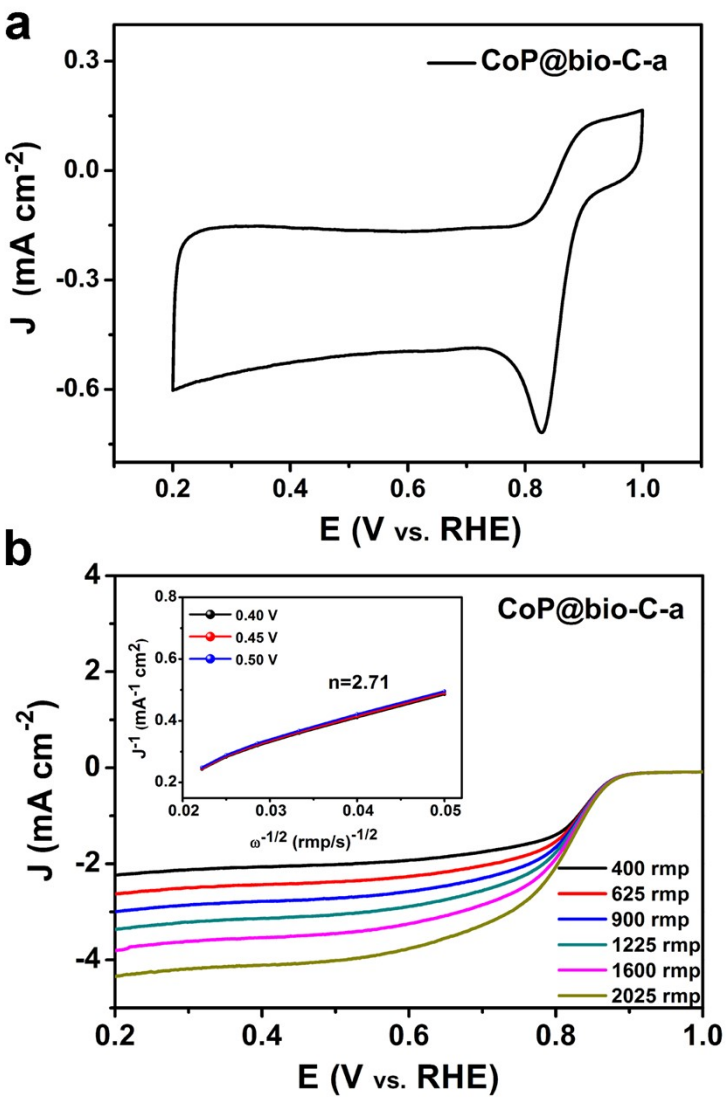

Figure S8. (a) CV and (b) LSV curves of CoP@bio-C-a catalyst in O_2-saturated 0.1 M KOH, respectively. (Inset: K–L plots of CoP@bio-C-a at various potentials.)

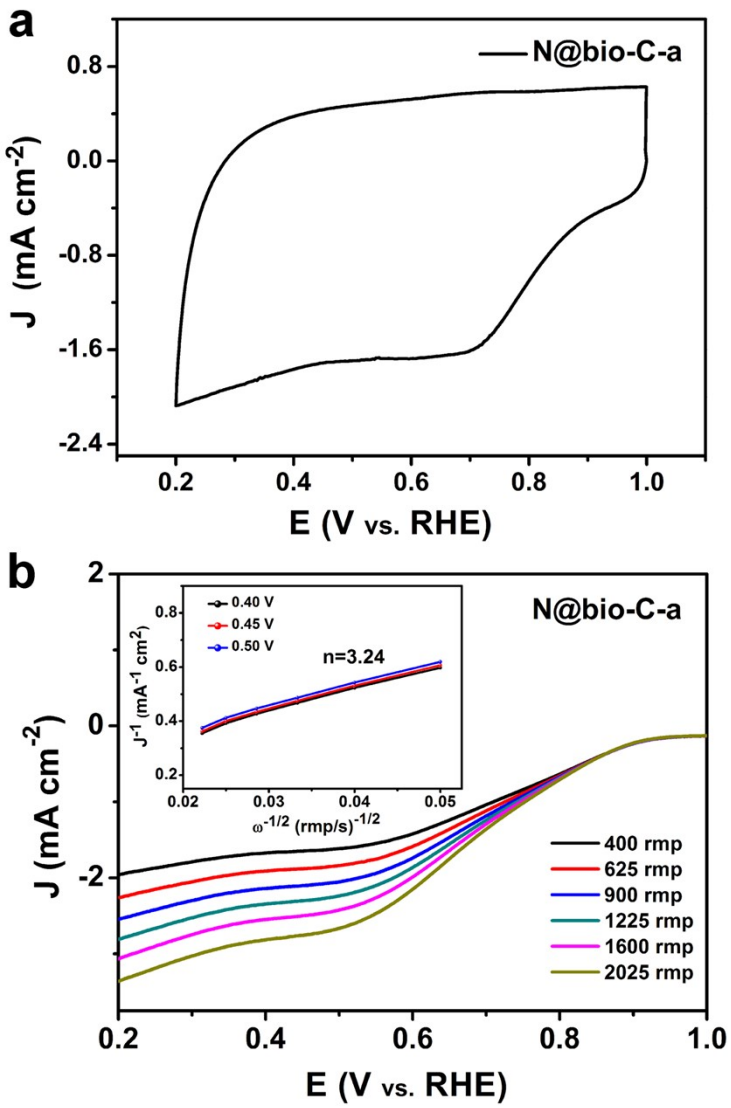

Figure S9. (a) CV and (b) LSV curves of N@bio-C-a catalyst in O_2-saturated 0.1 M KOH, respectively. (Inset: K–L plots of N@bio-C-a at various potentials.)

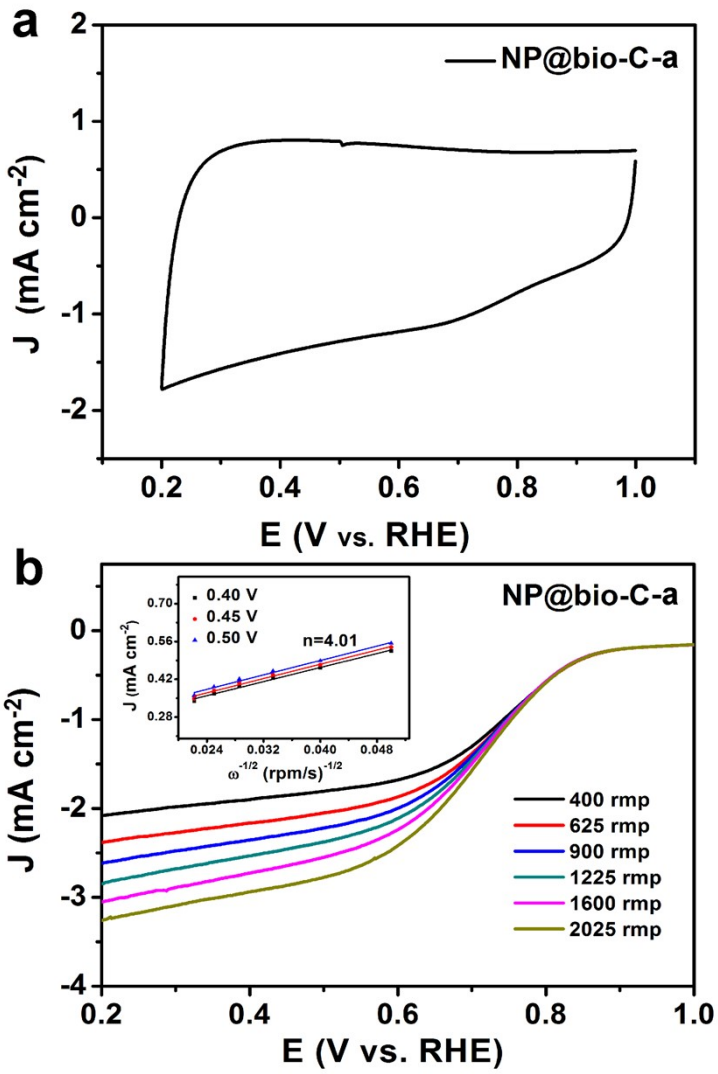

Figure S10. (a) CV and (b) LSV curves of NP@bio-C-a catalyst in O_2-saturated 0.1 M KOH, respectively. (Inset: K–L plots of NP@bio-C-a at various potentials.)

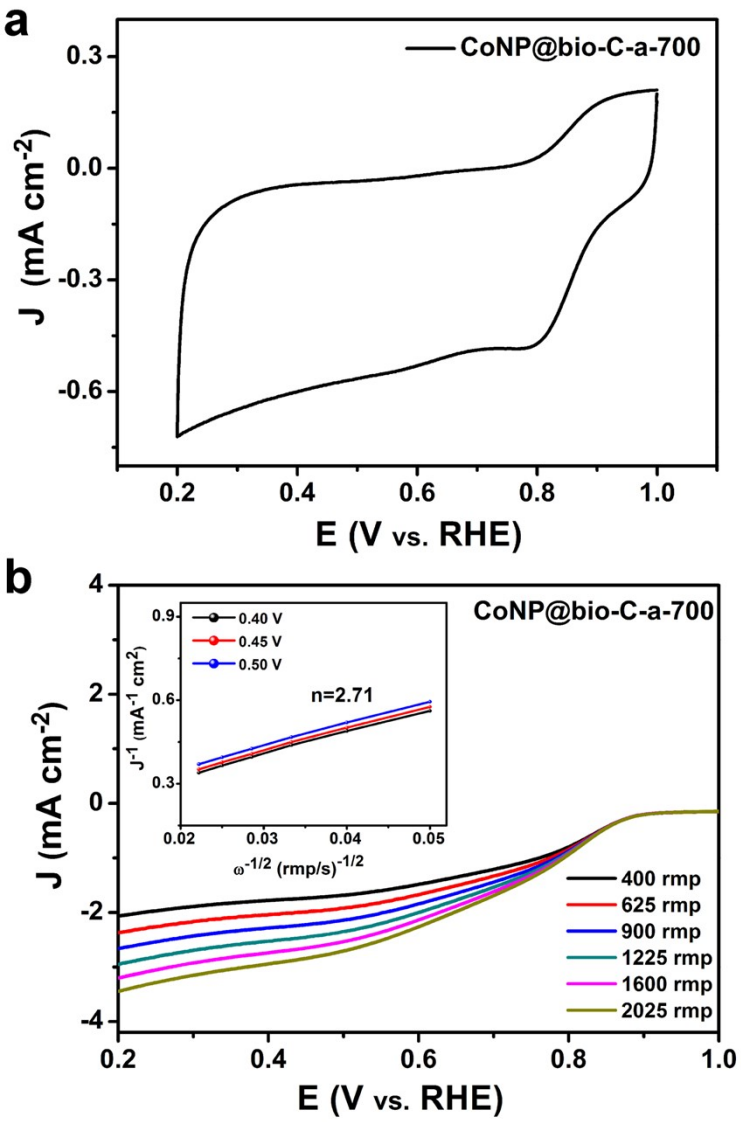

Figure S11. (a) CV and (b) LSV curves of CoNP@bio-C-a-700 catalyst in O_2-saturated 0.1 M KOH, respectively. (Inset: K–L plots of CoNP@bio-C-a-700 at various potentials.)

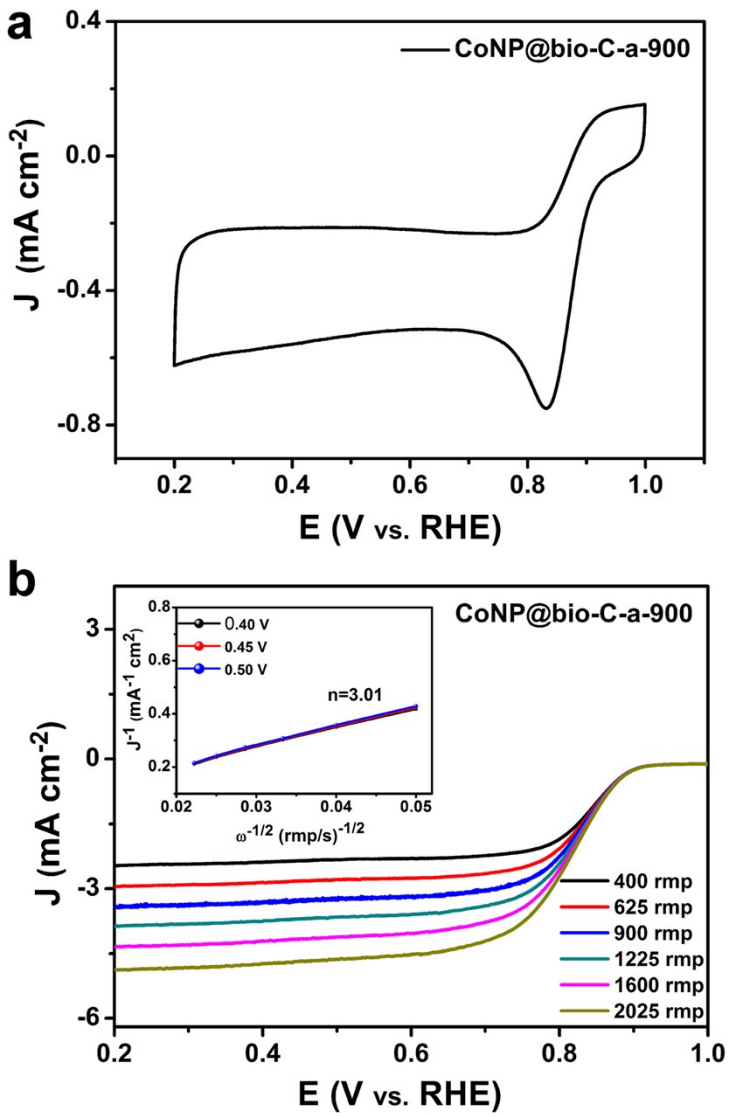

Figure S12. (a) CV and (b) LSV curves of CoNP@bio-C-a-900 catalyst in O_2-saturated 0.1 M KOH, respectively. (Inset: K–L plots of CoNP@bio-C-a-900 at various potentials.)

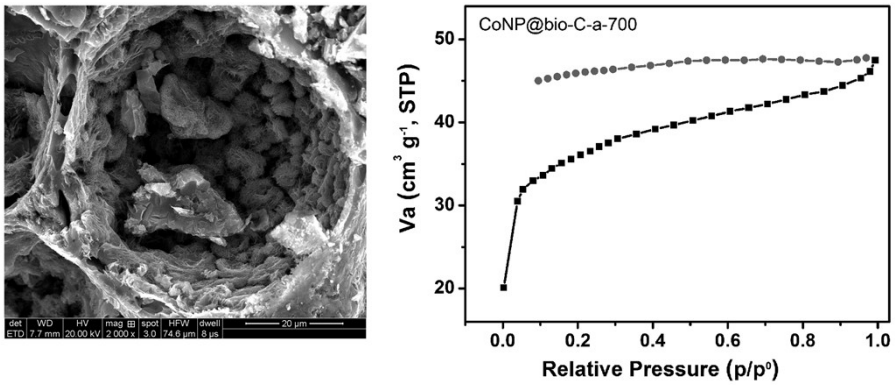

Figure S13. SEM image (left) and N_2 adsorption/desorption isotherms plot (right) of CoNP@bio-C-a-700 catalyst.

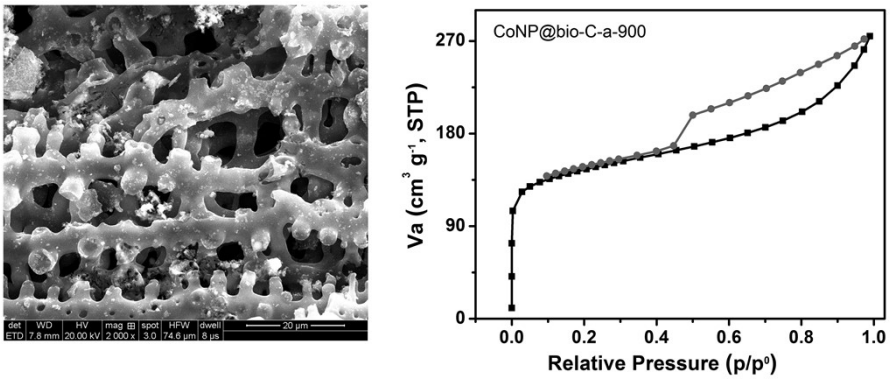

Figure S14. SEM image (left) and N_2 adsorption/desorption isotherms plot (right) of CoNP@bio-C-a-900 catalyst.

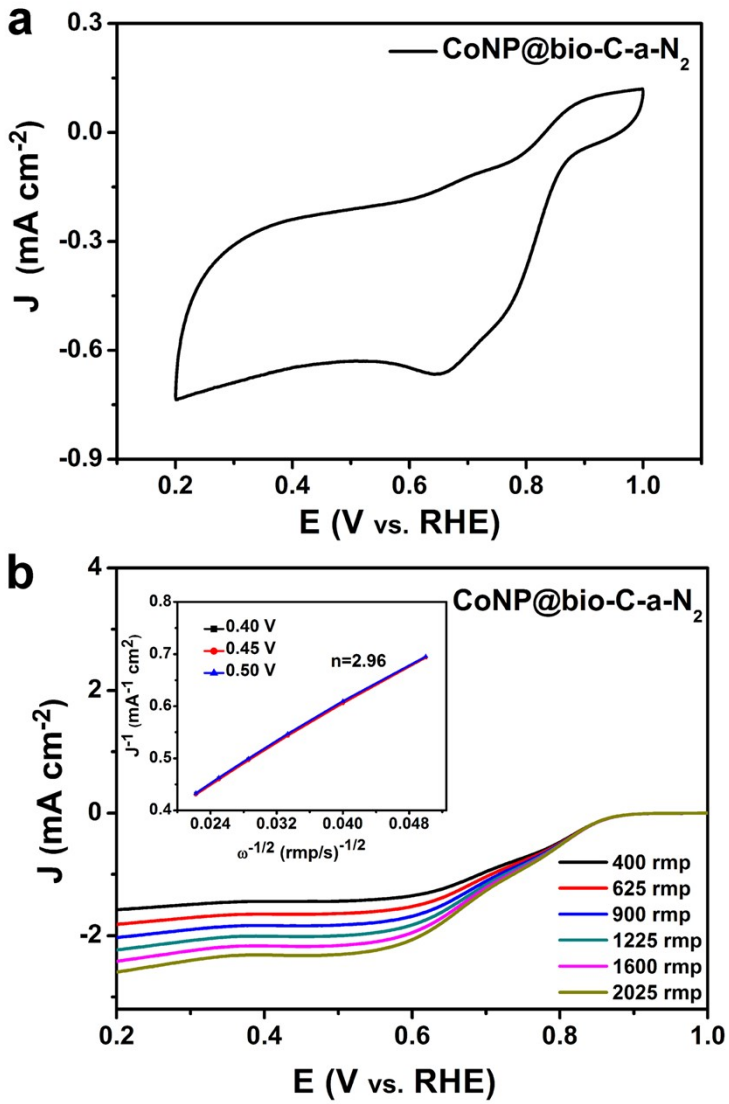

Figure S15. (a) CV and (b) LSV curves of CoNP@bio-C-a-N_2 catalyst in O_2-saturated 0.1 M KOH, respectively. (Inset: K–L plots of CoNP@bio-C-a-N_2 at various potentials.)

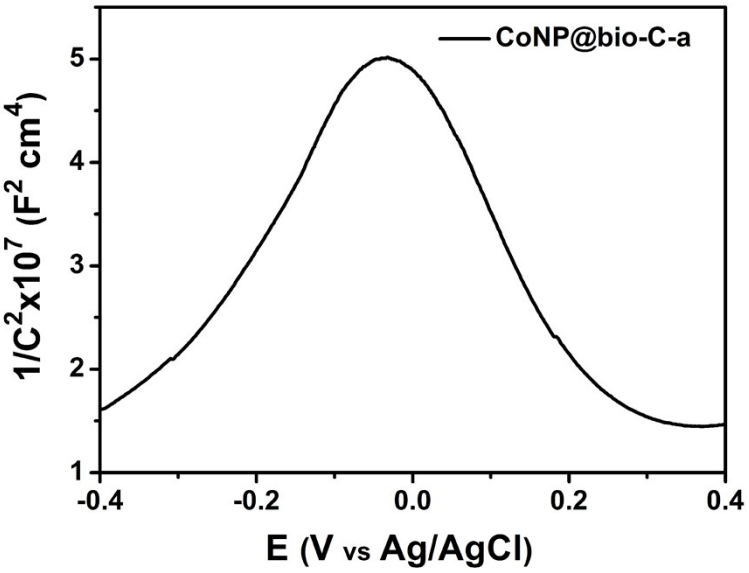

Figure S16. Mott–Schottky plots of the CoNP@bio-C-a at an AC frequency of 10 Hz.

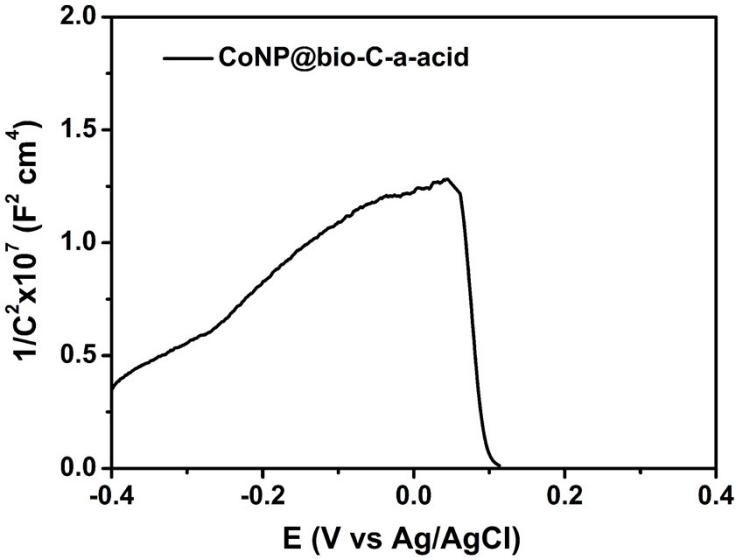

Figure S17. Mott–Schottky plots of the CoNP@bio-C-a-acid at an AC frequency of 10 Hz.

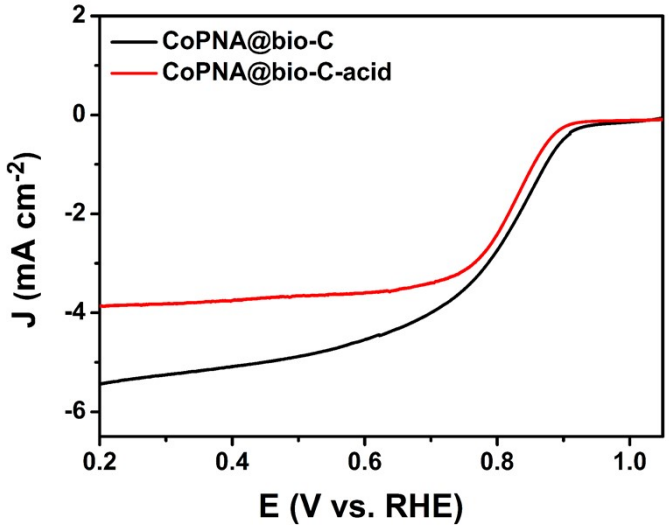

Figure S18. LSV curves of the CoNP@bio-C-a before (black line) and after acid leaching (red line).

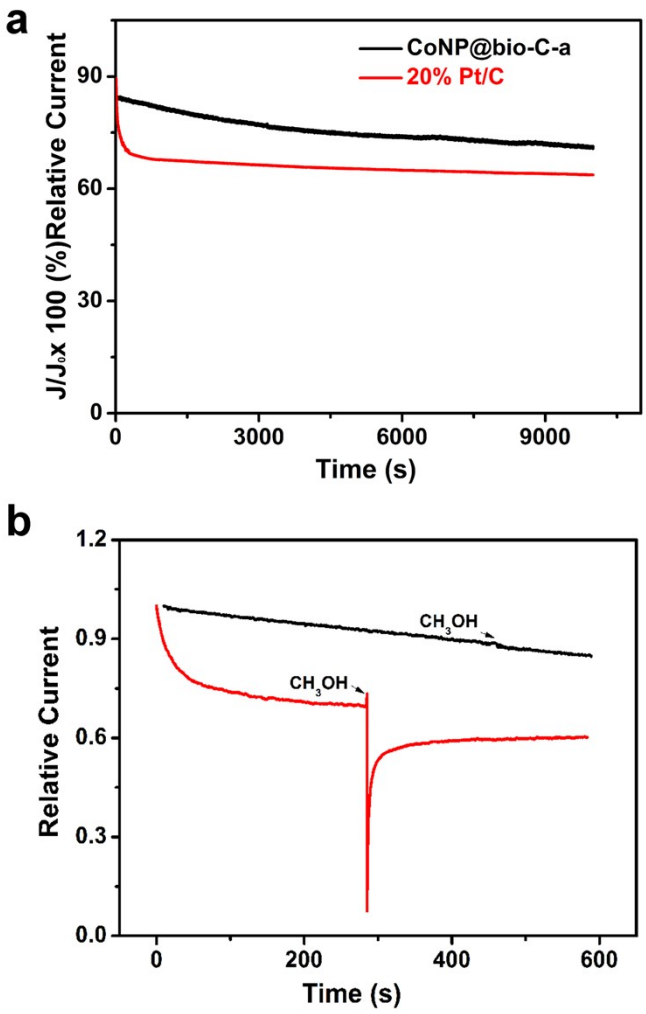

Figure S19. (a) Amperometric i–t curves of CoNP@bio-C-a and 20 wt% Pt/C and (b) upon the addition of 3 M methanol in O_2-saturated 0.1 M KOH solution with the rotation speed of 1600 rpm.

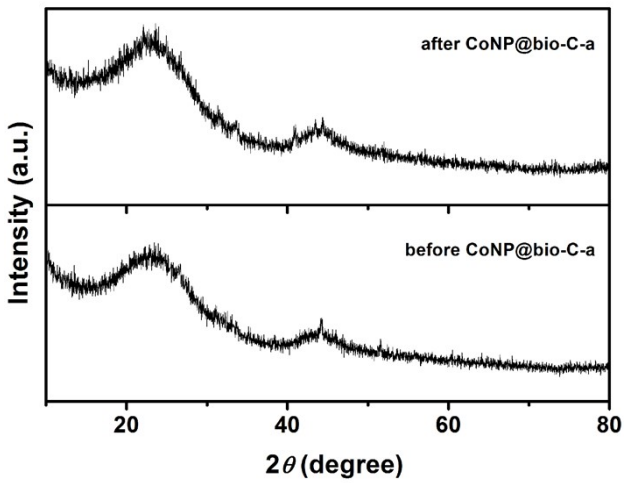

Figure S20. PXRD patterns of CoNP@bio-C-a catalyst before and after stability tests.

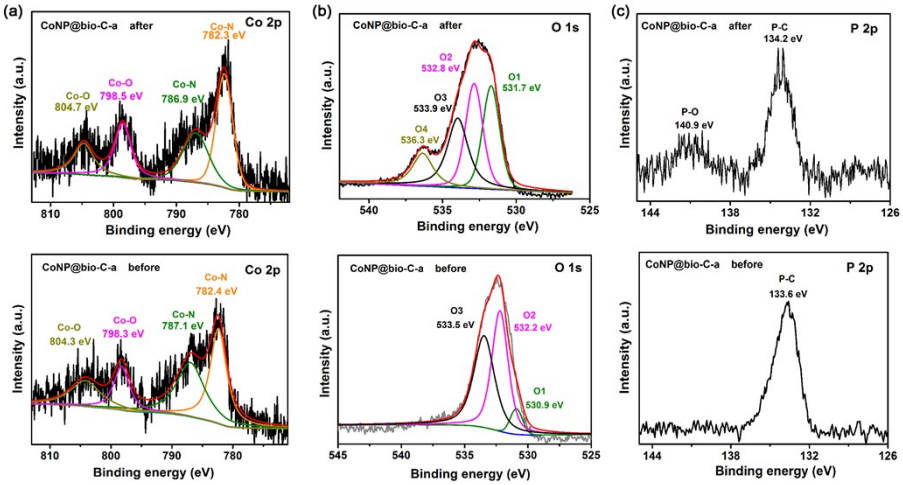

Figure S21. High-resolution XPS curves of the (a) Co 2p, and (b) O 1s, and (c) P 2p core levels for CoNP@bio-C-a catalyst before and after stability tests.

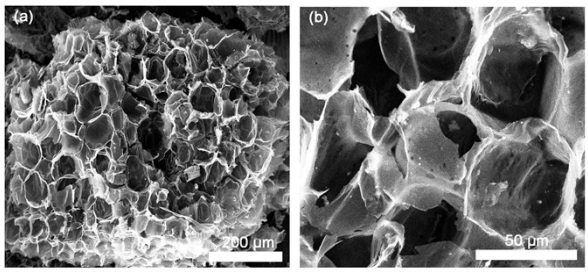

Figure S22. SEM images of CoNP@bio-C-a catalyst after stability tests.

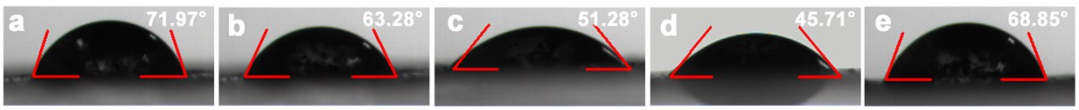

Figure S23. Contact angle measurements of (a) bio-C, (b) CoP@bio-C, (c) CoNP@bio-C, (d) CoNP@bio-C-a, and (e) N@bio-C-a using the electrolyte of distilled water.

Table S1. Composition (ICP-OES and EDX) of CoNP@bio-C-a catalysts.

Sample	Composition	
	ICP-OES	EDS
CoNP@bio-C-a	$Co_7:P_{18}$	$Co_3:P_8$

Table S2. The physical parameters of the bio-C, CoP@bio-C, CoNP@bio-C, and CoNP@bio-C-a under different tempreture, respectively.

Sample	Surface area (m^2 g^{-1})
bio-C	455.74
CoP@bio-C	291.82
CoNP@bio-C	365.40
CoNP@bio-C-a	475.55
CoNP@bio-C-a-700	128.96
CoNP@bio-C-a-900	499.62

Table S3. The ORR performance of the bio-C, CoP@bio-C, CoNP@bio-C, CoNP@bio-C-a, N@bio-C-a, NP@bio-C-a, and CoP@bio-C-a, CoNP@bio-C-a-700, CoNP@bio-C-a-900, CoNP@bio-C-a-N_2, in alkaline media at 1600 rpm, respectively.

Sample	E_{onset} (V)	$E_{1/2}$ (V)	J_L (mA cm^{-2})	n
bio-C	0.85	0.69/0.80	2.78	2.28
CoP@bio-C	0.85	0.79	3.47	2.37
CoNP@bio-C	0.89	0.82	3.84	2.87
CoNP@bio-C-a	0.92	0.85	5.49	4.06
N@bio-C-a	0.90	0.71	3.06	3.24
NP@bio-C-a	0.85	0.71	3.06	4.01
CoP@bio-C-a	0.89	0.83	3.77	2.71
CoP@bio-C-a-700	0.88	0.79	3.19	2.71
CoP@bio-C-a-900	0.91	0.83	4.34	3.01
CoNP@bio-C-a-N_2	0.86	0.65	2.41	2.96
20 wt% Pt/C	0.96	0.86	5.61	4.00

Table S4. Comparison of the ORR performance for CoNP@bio-C-a catalysts at 1600 rpm in 0.1 M KOH.

Catalysts	$E_{1/2}$ (V)	J_L (mA cm^{-2})	E_{onset} (V)	Tafel slope (mV dec^{-1})	n	Reference
CoNP@bio-C-a	0.85	5.49	0.92	--	4.06	This work
Co@Co_3O_4@C	0.78	4.65	0.90	--	--	*Energy Environ. Sci.*, 2015 [1]
Co@NG-acid	0.83	4.00	0.90	--	3.90	*Adv. Funct. Mater.*, 2016 [2]
Co-NC@CoP-NC	0.78	4.70	0.89	--	3.97	*J. Mater. Chem. A*, 2016 [3]
Co@Co_3O_4@PPD	0.78	4.20	0.90	--	3.78~3.96	*Small*, 2016 [4]
ZIF/rGO-700-AL	0.81	5.49	0.93	--	--	*J. Mater. Chem. A*, 2016 [5]
Co@NCNT	0.83	6.20	1.03	--	--	*J. Mater. Chem. A*, 2016 [6]
Co,N-CNF	0.85	5.71	0.92	60	4.00	*Adv. Mater.*, 2016 [7]
Cal-CoZIF-VXC72	0.84	5.92	--	35	4.00	*Adv. Mater.*, 2017 [8]
Co_3O_4/Co-N-C	0.91	5.10	0.98	68.5	3.62	*Journal of Power Sources*, 2017 [9]
NC@CoPx/PyCNTs-900	0.80	5.50	0.92	85	3.80	*Carbon*, 2018 [10]
Co/NPC	0.79	5.46	0.91	--	3.85~4.00	*J Mater Sci*, 2018 [11]
Co_3O_4/Co@N-G	0.81	5.20	0.96		3.91~3.96	*J. Mater. Chem. A*, 2019 [12]
CoP/NP-HPC	0.83	5.20	0.95	85	3.70	*J. Mater. Chem. A*, 2020 [13]

References

(1) Xia, W.; Zou, R. Q.; An, L.; Xia, D. G.; Guo, S. J. Metal-organic framework route to in-situ encapsulation of Co@Co_3O_4@C core@bishell nanoparticles into highly ordered porous carbon matrix for oxygen reduction. *Energy Environ. Sci.* **2015**, 8, 568–576.

(2) Zeng, M.; Liu, Y. L.; Zhao, F. P.; Nie, K. Q.; Han, N.; Wang, X. X.; Huang, W. J.; Song, X. N.; Zhong, J.; Li, Y. G. Metallic cobalt nanoparticles encapsulated in nitrogen enriched graphene shells: Its bifunctional electrocatalysis and application in Zinc–Air batteries. *Adv. Funct. Mater.* **2016**, 26, 4397–4404.

(3) Li, X. Y.; Jiang, Q. Q.; Dou, S.; Deng, L. B.; Huo, J.; Wang, S. Y. ZIF-67-derived Co-NC@CoP-NC nanopolyhedra as an efficient bifunctional oxygen electrocatalyst. *J. Mater. Chem. A* **2016**, 4, 15836–15840.

(4) Wang, Z. j.; Li, B.; Ge, X. M.; Thomas Goh, F. W.; Zhang, X.; Du, G. J.; Wuu, D.; Liu, Z. L.; Andy Hor, T. S.; Zhang, H.; Zong, Y. Co@Co_3O_4@PPD core@bishell nanoparticle-based composite as an efficient electrocatalyst for oxygen reduction reaction. *Small* **2016**, 12, 2580–2587.

(5) Wei, J.; Hu, Y. X.; Wu, Z. X.; Liang, Y.; Leong, S.; Kong, B.; Zhang, X. Y.; Zhao, D. Y.; Simon, G. P.; Wang, H. T. A graphene-directed assembly route to hierarchically porous Co-Nx/C catalysts for highperformance oxygen reduction. *J. Mater. Chem. A* **2015**, 3, 16867–16873.

(6) Zhang, E.; Xie, Y.; Ci, S. Q.; Jia, J. C.; Cai, P. W.; Yi, L. C.; Wen, Z. H. Multifunctional high-activity and robust electrocatalyst derived from metal-organic frameworks. *J. Mater. Chem. A* **2016**, 4, 17288–17298.

(7) Shang, L.; Yu, H. J.; Huang, X.; Bian, T.; Shi, R.; Zhao, Y. F.; Waterhouse, G. I. N.; Wu, L. Z.; Tung, C. H.; Zhang, T. R. Well-dispersed ZIF-derived Co,N-Co-doped carbon nanoframes through mesoporous-silica-protected calcination as efficient oxygen reduction electrocatalysts. *Adv. Mater.* **2016**, 28, 1668–1674.

(8) Ni, B.; Ouyang, C.; Xu, X. B.; Zhuang, J.; Wang, X. Modifying commercial carbon with trace amounts of ZIF to prepare derivatives with superior ORR activities. *Adv. Mater.* **2017**, 29, 1701354.

(9) Li, J. S.; Zhou, Z.; Liu, K.; Li, F. Z.; Peng, Z. G.; Tang, Y. G.; Wang, H. Y. Co_3O_4/Co-N-C modified ketjenblack carbon as an advanced electrocatalyst for Al-Air batteries. *Journal of Power Sources* **2017**, 343, 30–38.

(10) Wang, Q.; Fan, Y.; Wang, K. K.; Shen, H. M.; Li, G. J.; Fu, H. Y.; She, Y. B. Hierarchical tubular structures composed of CoPx and carbon nanotubes: Highly effective electrocatalyst for oxygen reduction. *Carbon* **2018**, 130, 241–249.
(11) Zhan, T. R.; Lu, S. S.; Rong, H. Q.; Hou, W. G.; Teng, H. N.; Wen, Y. H. Metal-organic-framework-derived Co/nitrogen-doped porous carbon composite as an effective oxygen reduction electrocatalyst. *Journal of Materials Science* **2018**, 53, 6774–6784.
(12) Guo, J.; Gadipelli, S.; Yang, Y. C.; Li, Z. N.; Lu, Y.; Brett, D. J. L.; Guo, Z. X. An efficient carbon-based ORR catalyst from low temperature etching of ZIF-67 with ultra-small cobalt nanoparticles and high yield. *J. Mater. Chem. A* **2019**, 7, 3544–3551.
(13) Wang,Y. X.; Wu, M. J.; Li, J.; Huang, H. T.; Qiao J. L. In-situ growth of CoP nanoparticles anchored on (N, P) co-doped porous carbon engineered by MOFs as advanced bifunctional oxygen catalyst for rechargeable Zn-air battery. *J. Mater. Chem. A* **2020**, 8, 19043–19049.